Pergamon

Int. J. Heat Mass Transfer. Vol. 39, No. 18, pp. 3911–3924, 1996

0017–9310/96 $15.00 + 0.00

PII: S0017–9310(96)00055–5

Modelling of a thermo-viscoelastic coupling for large deformations through finite element analysis

G. BÉRARDI, M. JAEGER and R. MARTIN

Institut Universitaire des Systèmes Thermiques Industriels, CNRS UA 1168, Av. Escadrille Normandie-Niemen, 13397 Marseille, Cedex 13, France

and

C. CARPENTIER

Unité modèles numériques, LMA-LMT, Technopole de Château Gombert, 13451 Marseille, Cedex 20, France

(*Received* 4 *November* 1994 *and in final form* 12 *January* 1996)

Abstract—In this article we present the mathematical model leading to the equations of the thermo-viscoelastic coupling for large deformations. We have chosen a Poynting–Thomson model to describe the rheological behavior of the material. In this model the source term generated by viscous frictions is independent of temperature. The two-dimensional heat transfer equation in Lagrangian form is solved via a finite element method for a two-layer elastomer-metal test piece under a shear force. The results of the numerical model are compared with experimental results which show that the source term cannot be temperature independent. For a more accurate description of the real behavior of the material the source term is then identified from experimental results via an inverse method. The numerical results agree well with the experimental ones. Copyright © 1996 Elsevier Science Ltd.

INTRODUCTION

Many industrial sectors, for example the automobile and aeronautic industries, use elastomers. In many cases they are used for pieces strictly linked to safety and are submitted to strong mechanical and thermal forces. However, the mechanical properties of elastomers strongly depend on temperature and when these materials are brought to low temperatures, their mechanical properties are perturbed by the onset of a glass transition which causes their stiffness to increase dramatically. This stiffness is accompanied by an internal heat dissipation occurring because of the increase in viscosity around the glass transition. The resulting heating alters the mechanical behavior of the elastomer and generates a new modification of the dissipation. Also, the absence of cooling may cause the appearance of hot points causing damage to the material. It is therefore necessary to know the thermo-mechanical behavior of these elastomers in order to predict the load limit and lifetime of these pieces.

Among the behavior aspects to be considered we can quote:

- hyperelasticity applied in quasi-state loading;
- thermo-viscoelasticity coupling to study the fatigue behavior for cyclic loading with large deformations.

Hyperelasticity has been the topic of several works. In contrast, less work has been conducted on viscoelasticity under large deformations. Among the currently used approaches for elastomers the statistical approach should be mentioned. It describes the material behavior from the behavior of molecular chains, i.e. their orientations, movements and constraints [1]. The microscopical numerical modelling is then tricky [2]. Another approach is the phenomenological approach which is based on experimental observations to model the internal energy and the material behaviour law. Several authors have proposed viscoelastic behaviour laws for finite deformations (up to about 100% deformation). Among these laws are integral behaviour laws which describe the constraints through a function of the deformation tensor at time t and a 'memory of deformations' tensor which accounts for the contributions of previous times [3].

As far as thermo-viscoelasticity is concerned, most works deal with the study of heating within structures submitted to plane harmonic deformations. These deformations are weak enough to describe the material behaviour through complex characteristics with respect to temperature and frequency [4–7]. Other works have been carried out in the same way to obtain the deformation and temperature field of

NOMENCLATURE

$\bar{\mathbf{A}}(\mathbf{X}, t)$	Almansi–Euler deformation tensor	Cof $\bar{\mathbf{C}}_v$	$\det \bar{\mathbf{C}}_v\, \bar{\mathbf{C}}_v^{-1}$
$\bar{\mathbf{C}}(\mathbf{X}^0, t)$	right Cauchy–Green tensor	$s(\mathbf{X}^0, t)$	entropy
Cp	heat capacity	$\bar{\mathbf{S}}(\mathbf{X}^0, t)$	second Piola–Kirchoff stress tensor
$\bar{\mathbf{D}}(\mathbf{X}, t)$	tensor of deformation rates	$T(\mathbf{X}, t)$	temperature
$\bar{\mathbf{E}}(\mathbf{X}^0, t)$	Green–Lagrange deformation tensor	$\mathbf{U}$	derivative according to time of position vector
$e(\mathbf{X}, t)$	internal energy	$\mathbf{X}$	position vector of point X
f	frequency	$\mathbf{X}^0$	initial position vector of point X.
$\bar{\mathbf{F}}(\mathbf{X}^0, t)$	gradient tensor	Greek symbols	
$\bar{\mathbf{K}}(T)$	conductivity tensor	λ	conductivity
$\mathbf{q}(\mathbf{X}, t)$	density of the heat flux	$\bar{\mathbf{\Pi}}(\mathbf{X}^0, t)$	first Piola–Kirchoff stress tensor
$r(\mathbf{X}, t)$	production rate of energy	$\rho(\mathbf{X}, t)$	density
Cof $\bar{\mathbf{F}}$	$\det \bar{\mathbf{F}}\, \bar{\mathbf{F}}^{-1}$	$\bar{\mathbf{\Sigma}}(\mathbf{X}, t)$	Cauchy stress tensor.

materials submitted to mechanical and thermal loadings, but for small deformations [8,9].

We are using here an approach which generalizes a simple rheological model (Poynting–Thomson) to large deformations [10,11], so that the results can be applied to a larger number of cases.

From the basic relations of the mechanics of a continuous media, we present an approach to obtain the equations governing the viscoelastic behaviour and in particular the energy equation for large deformations. In the latter, a source term appears which depends on the physical parameters characterizing the mechanical behaviour of the body and which represents the quantity of energy dissipated by internal dumping. Continuum equations for the finite element simulation are written in Lagrangian form utilizing the initial configuration as the reference state.

In this article, we first briefly describe the mechanical problem for large deformations. From the basic principle of thermodynamics of continuous media, we then present the mathematical model which enables us to obtain the equations governing the thermo-viscoelastic behaviour. Finally, we focus on the energy equation and solve it via a finite element method. Our approach is validated by treating a two-layer elastomer-metal test piece being sheared. As this mechanical problem has an analytical solution, it provides a good benchmark problem.

1. DESCRIPTION OF THE MECHANICAL PROBLEM

1.1. *Description of the kinematics*

Because of their low modulus of elasticity and of their viscous properties, rubber elastomers are used more and more to manufacture articulated or damping pieces. These pieces may be subjected to very strong mechanical loadings (traction, shearing, torsion, deflection...) generating large deformations of the elastomer. The theory of small deformations is not appropriate for the description of the behaviour of these materials. It is therefore necessary to distinguish an initial or reference configuration from the deformed or present configuration, which is unnecessary in small deformations (Fig. 1).

We use a Lagrangian description of the movement. In finite element modelling, the mesh deforms itself in time when the thermo-viscoelastic coupling is solved in the deformed configuration. Therefore, we have opted for the reference configuration to avoid any remeshing or element degeneration problems.

At each time the movement is thus defined in a Cartesian coordinate system by three equations such as $x_i = x_i(x_1^0, x_2^0, x_3^0, t)$, $i = 1,2,3$, where (x_1, x_2, x_3) represent the coordinates of point X in the current configuration and (x_1^0, x_2^0, x_3^0) the coordinates of the same point X in the reference configuration. We will denote by $\mathbf{X}$ the position vector of the point in the current configuration and $\mathbf{X}^0$ the position vector of the point in the reference configuration. The local behaviour of the media during the movement is characterized by the tangent linear mapping, or gradient tensor, $\bar{\mathbf{F}}(\bar{\mathbf{X}}^0, t)$, whose components are defined by

$$F_{ij} = \frac{\partial x_i}{\partial x_j^0}.$$

This tensor is used to obtain the appropriate transformation relations for the length, surface and volume elements between the two configurations [12–14]

$$\mathrm{d}\mathbf{X} = \bar{\mathbf{F}}(\bar{\mathbf{X}}^0, t)\,\mathrm{d}\mathbf{X}^0 \tag{1a}$$

$$\mathbf{N}(\mathbf{X}, t)\,\mathrm{d}S = \det \bar{\mathbf{F}}(\mathbf{X}^0, t)\bar{\mathbf{F}}^{-\mathrm{T}}(\mathbf{X}^0, t)\mathbf{N}^0(\mathbf{X}^0, t)\,\mathrm{d}S^0 \tag{1b}$$

$$\mathrm{d}V = \det \bar{\mathbf{F}}(\mathbf{X}^0, t)\,\mathrm{d}V^0. \tag{1c}$$

Deformations. From tensor $\bar{\mathbf{F}}(\mathbf{X}^0, t)$, it is possible to define two deformation tensors [12], the Green–Lagrange deformation tensor $\bar{\mathbf{E}}(\mathbf{X}^0, t)$ in the reference

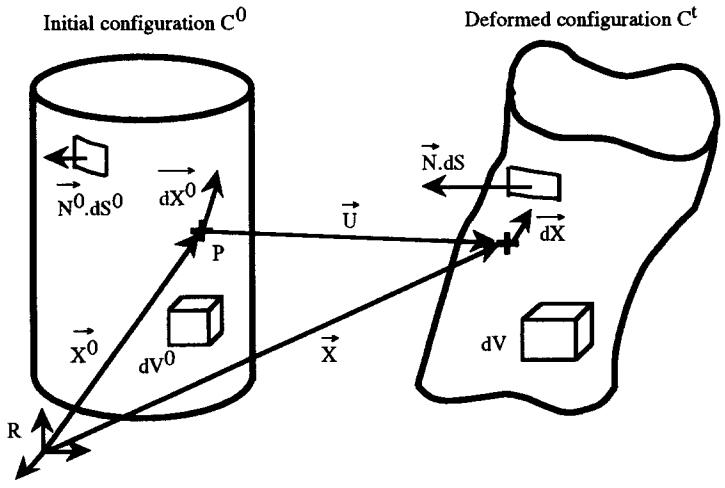

Fig. 1. Initial configurations and deformed configuration.

configuration and the Almansi–Euler deformation tensor $\bar{\mathbf{A}}(\mathbf{X}^0, t)$ in the deformed configuration

$$\bar{\mathbf{E}}(\mathbf{X}^0, t) = \tfrac{1}{2}(\bar{\mathbf{F}}^{\mathrm{T}}(\mathbf{X}^0, t)\bar{\mathbf{F}}(\mathbf{X}^0, t) - \bar{\mathbf{I}})$$

$$\text{and} \quad \bar{\mathbf{A}}(\mathbf{X}, t) = \tfrac{1}{2}(\bar{\mathbf{I}} - (\bar{\mathbf{F}}(\mathbf{X}^0, t)\bar{\mathbf{F}}^{\mathrm{T}}(\mathbf{X}^0, t))^{-1}).$$

We also introduce the dilatation tensor or right Cauchy–Green tensor, defined by

$$\bar{\mathbf{C}}(\mathbf{X}^0, t) = \bar{\mathbf{F}}^{\mathrm{T}}(\mathbf{X}^0, t)\bar{\mathbf{F}}(\mathbf{X}^0, t).$$

Deformation velocity. In order to characterize velocities, we introduce the vector $\mathbf{U}$, time derivative of the position vector $\mathbf{X}(\mathbf{X}^0, t)$, in the current configuration

$$\mathbf{U} = \left\{\frac{\mathrm{d}\mathbf{X}}{\mathrm{d}t}\right\} = \dot{\bar{\mathbf{F}}}(\mathbf{X}^0, t)\{\mathrm{d}\mathbf{X}^0\} = \bar{\mathbf{L}}(\mathbf{X}, t)\{\mathrm{d}\mathbf{X}\}$$

$$\text{with:} \quad \bar{\mathbf{L}}(\mathbf{X}, t) = \dot{\bar{\mathbf{F}}}(\mathbf{X}^0, t)\bar{\mathbf{F}}^{-1}(\mathbf{X}^0, t).$$

By utilizing the relationship $\langle \mathrm{d}\mathbf{X}\rangle\{\mathrm{d}\mathbf{Y}\} - \langle \mathrm{d}\mathbf{X}^0\rangle \{\mathrm{d}\mathbf{Y}^0\} = 2\langle \mathrm{d}\mathbf{X}^0\rangle\bar{\mathbf{E}}(\mathbf{X}^0, t)\{\mathrm{d}\mathbf{Y}^0\}$ we obtain

$$\frac{\mathrm{d}}{\mathrm{d}t}(\langle \mathrm{d}\mathbf{X}\rangle\{\mathrm{d}\mathbf{Y}\}) = 2\langle \mathrm{d}\mathbf{X}^0\rangle\dot{\bar{\mathbf{E}}}(\mathbf{X}^0, t)\{\mathrm{d}\mathbf{Y}^0\}.$$

However, this expression can also be obtained as follows:

$$\frac{\mathrm{d}}{\mathrm{d}t}(\langle \mathrm{d}\mathbf{X}\rangle\{\mathrm{d}\mathbf{Y}\}) = \langle \mathrm{d}\mathbf{X}\rangle(\bar{\mathbf{L}}^{\mathrm{T}}(\mathbf{X}, t) + \bar{\mathbf{L}}(\mathbf{X}, t))\{\mathrm{d}\mathbf{Y}\} = 2\langle \mathrm{d}\mathbf{X}\rangle\bar{\mathbf{D}}(\mathbf{X}, t)\{\mathrm{d}\mathbf{Y}\}.$$

The tensor of deformation rates, $\bar{\mathbf{D}}(\mathbf{X}, t)$, can also be expressed by the symmetric part of tensor $\bar{\mathbf{L}}(\mathbf{X}, t)$. The deformation velocity, which has been expressed in terms of $\bar{\mathbf{D}}(\mathbf{X}, t)$ in the deformed configuration, is expressed in terms of $\dot{\bar{\mathbf{E}}}(\mathbf{X}^0, t)$ in the reference configuration. Both tensors are related by

$$\dot{\bar{\mathbf{E}}}(\mathbf{X}^0, t) = \bar{\mathbf{F}}^{\mathrm{T}}(\mathbf{X}^0, t)\bar{\mathbf{D}}(\mathbf{X}, t)\bar{\mathbf{F}}(\mathbf{X}^0, t).$$

1.2. *Description of stress*

In the deformed configuration, the constraint state is described by Cauchy stress tensor, $\bar{\mathbf{\Sigma}}(\mathbf{X}, t)$, which produces stress vector $\mathbf{T}(\mathbf{X}, t)$ acting on a surface element with normal $\mathbf{N}(\mathbf{X}, t)$. The local contact force is then

$$\mathrm{dt}(\mathbf{X}, t) = \mathbf{T}(\mathbf{X}, t)\,\mathrm{d}S = \bar{\mathbf{\Sigma}}(\mathbf{X}, t)\mathbf{N}(\mathbf{X}, t)\,\mathrm{d}S.$$

Using equation (1b) it can be written as

$$\mathrm{dt}(\mathbf{X}, t) = \det\bar{\mathbf{F}}(\mathbf{X}^0, t)\bar{\mathbf{\Sigma}}(\mathbf{X}, t)\bar{\mathbf{F}}^{-\mathrm{T}}(\mathbf{X}^0, t)\mathbf{N}^0(\mathbf{X}^0, t)\,\mathrm{d}S^0 = \bar{\mathbf{\Pi}}(\mathbf{X}^0, t)\mathbf{N}^0(\mathbf{X}^0, t)\,\mathrm{d}S^0,$$

where $\bar{\mathbf{\Pi}}(\mathbf{X}^0, t)$ is the first Piola–Kirchoff stress tensor. This tensor expresses at time t the contact force exerted on a surface element of the initial configuration. Lastly, the description of the local contact force related to the reference configuration is

$$\mathrm{dt}^0(\mathbf{X}^0, t) = \bar{\mathbf{F}}^{-1}(\mathbf{X}^0, t)\bar{\mathbf{\Pi}}(\mathbf{X}^0, t)\mathbf{N}^0(\mathbf{X}^0, t)\,\mathrm{d}S^0 = \bar{\mathbf{S}}(\mathbf{X}^0, t)\mathbf{N}^0(\mathbf{X}^0, t)\,\mathrm{d}S^0$$

$$\text{since:} \quad \mathrm{dt}^0(\mathbf{X}^0, t) = \bar{\mathbf{F}}^{-1}(\mathbf{X}^0, t)\,\mathrm{dt}(\mathbf{X}, t).$$

Here the symmetric tensor $\bar{\mathbf{S}}(\mathbf{X}^0, t)$ is the second Piola–Kirchoff stress tensor. The relationship between the three tensors is given by

$$\det\bar{\mathbf{F}}(\mathbf{X}^0, t)\bar{\mathbf{\Sigma}}(\mathbf{X}, t) = \bar{\mathbf{\Pi}}(\mathbf{X}^0, t)\bar{\mathbf{F}}^{\mathrm{T}}(\mathbf{X}^0, t) = \bar{\mathbf{F}}(\mathbf{X}^0, t)\mathbf{S}(\mathbf{X}^0, t)\bar{\mathbf{F}}^{\mathrm{T}}(\mathbf{X}^0, t). \quad (2)$$

1.3. *Equations of the mechanical problem*

Equation of mass conservation. With the aid of equation (1) the mass in an elemental volume is

$$\rho^0(\mathbf{X}^0, t)\,\mathrm{d}V^0 = \rho(\mathbf{X}, t)\,\mathrm{d}V = \rho(\mathbf{X}, t)\det\bar{\mathbf{F}}(\mathbf{X}^0, t)\,\mathrm{d}V^0,$$

where $\rho^0(\mathbf{X}^0, t)$ represents the local density in the initial configuration and $\rho(\mathbf{X}, t)$ the local density in the deformed configuration. In the mechanical study of elastomers, the incompressibility assumption has generally been used successfully. This assumption expresses $\rho^0(\mathbf{X}^0, t) = \rho(\mathbf{X}, t)$, that is

$$\frac{\mathrm{d}V}{\mathrm{d}V^0} = \frac{\rho^0(\mathbf{X}^0, t)}{\rho(\mathbf{X}, t)} = \det \bar{\mathbf{F}}(\mathbf{X}^0, t) = 1. \tag{3}$$

Conservation of momentum. If $\mathbf{f}(\mathbf{X}, t)$ is a force per unit volume describing the action of distant forces and $\mathbf{T}(\mathbf{X}, t)$ is the stress vector, the conservation of momentum in the present configuration is

$$\frac{\mathrm{d}}{\mathrm{d}t}\int_{D(t)} \rho(\mathbf{X}, t) U_i(\mathbf{X}, t)\,\mathrm{d}V - \int_{\partial D(t)} T_i(\mathbf{X}, t)\,\mathrm{d}S = \int_{D(t)} f_i(\mathbf{X}, t)\,\mathrm{d}V.$$

where $U_i(\mathbf{X}, t)$ represents the components of the velocity field $\mathbf{U}(\mathbf{X}, t)$ in the domain $D(t)$. By using the previous relations and assuming incompressibility, we obtain the Lagrangian form of this equation in the reference configuration

$$\frac{\mathrm{d}}{\mathrm{d}t}\int_{D_0} \rho^0(\mathbf{X}^0, t) U_i(\mathbf{X}^0, t)\,\mathrm{d}V^0 - \int_{\partial D_0} \Pi_{ik}(\mathbf{X}^0, t) N_k^0(\mathbf{X}^0, t)\,\mathrm{d}S^0 = \int_{D_0} f_i(\mathbf{X}^0, t)\,\mathrm{d}V^0$$

to which corresponds the following local form:

$$\rho^0(X, t)\frac{\partial U_i(\mathbf{X}^0, t)}{\partial t} = \Pi_{ik,k}(\mathbf{X}^0, t) + f_i(\mathbf{X}^0, t).$$

2. THERMO-VISCOELASIC ASPECTS OF THE COUPLING

2.1. *Conservation of energy*

The equation of conservation of energy usually written in Eulerian variables in the current configuration is

$$\frac{\mathrm{d}}{\mathrm{d}t}\int_{D(t)} \rho(\mathbf{X}, t) e(\mathbf{X}, t)\,\mathrm{d}V = \int_{D(t)} (r(\mathbf{X}, t) + \bar{\boldsymbol{\Sigma}}(\mathbf{X}, t) : \bar{\mathbf{D}}(\mathbf{X}, t))\,\mathrm{d}V - \int_{\partial D(t)} \langle \mathbf{q}(\mathbf{X}, t)\rangle \{\mathbf{N}(\mathbf{X}, t)\}\,\mathrm{d}S.$$

where $e(\mathbf{X}, t)$ represents the internal energy, $r(\mathbf{X}, t)$ the production rate of energy supplied from outside and $\mathbf{q}(\mathbf{X}, t)$ the heat flux by conduction. The latter is related to temperature by Fourier law

$$\mathbf{q}(\mathbf{X}, t) = -\bar{\mathbf{K}}(T)\mathbf{grad}(T(\mathbf{X}, t)),$$

where $\mathbf{K}(T)$ is the thermal conductivity tensor of the material, and $\bar{\boldsymbol{\Sigma}}(\mathbf{X}, t) : \bar{\mathbf{D}}(\mathbf{X}, t)$ describes the internal production of energy resulting from the viscous friction. By using the previous relations and assuming incompressibility, this equation becomes

$$\frac{\mathrm{d}}{\mathrm{d}t}\int_{D^0} \rho^0(\mathbf{X}^0, t) e(\mathbf{X}^0, t)\,\mathrm{d}V^0 = \int_{D^0}\left(r(\mathbf{X}^0, t) + \bar{\mathbf{S}}(\mathbf{X}^0, t) : \frac{\mathrm{d}\bar{\mathbf{E}}(\mathbf{X}^0, t)}{\mathrm{d}t}\right)\mathrm{d}V^0 - \int_{\partial D^0} \langle \mathbf{q}(\mathbf{X}, t)\rangle \bar{\mathbf{F}}^{-\mathrm{T}}(\mathbf{X}^0, t)\{\mathbf{N}^0(\mathbf{X}^0, t)\}\,\mathrm{d}S^0.$$

Defining the heat flux in the reference configuration by

$$\mathbf{Q}(\mathbf{X}^0, t) = \bar{\mathbf{F}}^{-1}(\mathbf{X}^0, t)\mathbf{q}(\mathbf{X}, t).$$

The conservation of energy equations in this configuration finally is

$$\frac{\mathrm{d}}{\mathrm{d}t}\int_{D^0} \rho^0(\mathbf{X}^0, t) e(\mathbf{X}^0, t)\,\mathrm{d}V^0 = \int_{D^0}\left(r(\mathbf{X}^0, t) + \bar{\mathbf{S}}(\mathbf{X}^0, t) : \frac{\mathrm{d}\bar{\mathbf{E}}(\mathbf{X}^0, t)}{\mathrm{d}t}\right)\mathrm{d}V^0 - \int_{\partial D^0} \langle \mathbf{Q}(\mathbf{X}^0, t)\rangle \{\mathbf{N}^0(\mathbf{X}^0, t)\}\,\mathrm{d}S^0.$$

The corresponding local equation is then

$$\rho^0(\mathbf{X}^0, t)\frac{\mathrm{d}e(\mathbf{X}^0, t)}{\mathrm{d}t} = r(\mathbf{X}^0, t) + \bar{\mathbf{S}}(\mathbf{X}^0, t) : \frac{\mathrm{d}\bar{\mathbf{E}}(\mathbf{X}^0, t)}{\mathrm{d}t} - \mathrm{div}(\mathbf{Q}(\mathbf{X}^0, t)). \tag{4}$$

2.2. *Dissipation*

Second principle of thermodynamics and Clausius–Duhem inequality. The second principle of thermodynamics expresses the evolution of entropy $s(\mathbf{X}^0, t)$ in the reference configuration as

$$\rho^0(\mathbf{X}^0, t)\frac{\mathrm{d}s(\mathbf{X}^0, t)}{\mathrm{d}t} \geqslant \int_{D^0} \frac{r(\mathbf{X}^0, t)}{T(\mathbf{X}^0, t)}\,\mathrm{d}V^0 - \int_{\partial D^0} \frac{\langle \mathbf{Q}(\mathbf{X}^0, t)\rangle \{\mathbf{N}^0(\mathbf{X}^0, t)\}}{T(\mathbf{X}^0, t)}\,\mathrm{d}S^0.$$

Expressing $r(\mathbf{X}^0, t)$ from equation (4) and using the relationship between free energy and internal energy ($e = \Psi + Ts$) leads to the Clausius–Duhem inequality. This inequality demonstrates that energy dissipation $\phi(\mathbf{X}^0, t)$ is positive or null

$$\phi(\mathbf{X}^0,t)=\bar{\mathbf{\Pi}}(\mathbf{X}^0,t):\mathbf{F}(\mathbf{X}^0,t)-\rho^0(\mathbf{X}^0,t)\times\left(\frac{\mathrm{d}\Psi(\mathbf{X}^0,t)}{\mathrm{d}t}+s(\mathbf{X}^0,t)\frac{\mathrm{d}T(\mathbf{X}^0,t)}{\mathrm{d}t}\right)-\frac{\langle\mathbf{Q}(\mathbf{X}^0,t)\rangle\{\mathbf{grad}(T(\mathbf{X}^0,t))\}}{T(\mathbf{X}^0,t)}\geqslant 0.$$

This dissipation is usually composed of an intrinsic dissipation $\phi_{\mathrm{int}}(\mathbf{X}^0,t)$ resulting from mechanical irreversibilities and a thermal dissipation $\phi_{\mathrm{th}}(\mathbf{X}^0,t)$ resulting from conductive heat transfer [12–16]

$$\phi_{\mathrm{int}}(\mathbf{X}^0,t)=\bar{\mathbf{\Pi}}(\mathbf{X}^0,t):\bar{\mathbf{F}}(\mathbf{X}^0,t)-\rho^0(\mathbf{X}^0,t)\times\left(\frac{\mathrm{d}\Psi(\mathbf{X}^0,t)}{\mathrm{d}t}+s(\mathbf{X}^0,t)\frac{\mathrm{d}T(\mathbf{X}^0,t)}{\mathrm{d}t}\right)\geqslant 0 \quad (5)$$

$$\phi_{\mathrm{th}}(\mathbf{X}^0,t)=-\frac{\langle\mathbf{Q}(\mathbf{X}^0,t)\rangle\{\mathbf{grad}(T(\mathbf{X}^0,t))\}}{T(\mathbf{X}^0,t)}\geqslant 0.$$

When assuming a decoupling of thermal and mechanical dissipative phenomena, both forms of dissipation must remain independently positive or null to satisfy the Clausius–Duhem inequality.

Intrinsic dissipation. The purpose here is to identify a rheological model in order to obtain a characterization of the dissipation process. This model must allow for the choice of:

- independent thermodynamic variables;
- a thermodynamic potential $\psi(\mathbf{X}^0,t)$;
- a dissipation potential $\varphi(\mathbf{X}^0,t)$.

For its admissibility the process must satisfy the previous inequalities [12, 15, 16]. Both potentials are expressed in terms of the independent variables.

To describe the thermo-viscoelastic behaviour, we assume there is an intermediate state which considers a multiplicative decomposition into an elastic and a nonelastic deformation. This approach, which is common in plasticity, has been used by many authors to set viscoelastic behaviour laws for large deformations [15–18]. We thus define a pseudo gradient of elastic deformation $\bar{\mathbf{F}}_{\mathrm{e}}(\mathbf{X}^0,t)$ and a pseudo gradient of viscoelastic deformation $\bar{\mathbf{F}}_{\mathrm{v}}(\mathbf{X}^0,t)$ such that

$$\bar{\mathbf{F}}(\mathbf{X}^0,t)=\bar{\mathbf{F}}_{\mathrm{e}}(\mathbf{X}^0,t)\bar{\mathbf{F}}_{\mathrm{v}}(\mathbf{X}^0,t).$$

A viscoelastic dilatation tensor $\bar{\mathbf{C}}_{\mathrm{v}}(\mathbf{X}^0,t)$ is associated with the pseudo gradient of viscoelastic deformation. This tensor is defined by

$$\bar{\mathbf{C}}_{\mathrm{v}}(\mathbf{X}^0,t)=\bar{\mathbf{F}}_{\mathrm{v}}^{\mathrm{T}}(\mathbf{X}^0,t)\bar{\mathbf{F}}_{\mathrm{v}}(\mathbf{X}^0,t).$$

Temperature $T(\mathbf{X}^0,t)$, the gradient tensor $\bar{\mathbf{F}}(\mathbf{X}^0t)$ and the viscoelastic dilatation tensor $\bar{\mathbf{C}}_{\mathrm{v}}(\mathbf{X}^0,t)$ then constitute a coherent choice for independent variables.

Furthermore, the potential for dissipation only depends on variables characterizing dissipation phenomena. The thermodynamic potential and the potential of dissipation are then given by

$$\psi(\mathbf{X}^0,t)=\psi(T,\bar{\mathbf{C}},\bar{\mathbf{C}}_{\mathrm{v}}) \quad \text{and} \quad \varphi(\mathbf{X}^0,t)=\varphi(\dot{\bar{\mathbf{C}}}_{\mathrm{v}},T).$$

Global incompressibility ($\det\bar{\mathbf{F}}=J_{\mathrm{F}}=1$) and local incompressibility ($\det\bar{\mathbf{C}}_{\mathrm{v}}=J_{\mathrm{v}}=1$) are taken into account through Lagrangian multipliers p and q. This leads us to replace the potential $\psi(T,\bar{\mathbf{C}},\bar{\mathbf{C}}_{\mathrm{v}})$ in the dissipation [equation (5)] with

$$\tilde{\psi}(T,\bar{\mathbf{C}},\bar{\mathbf{C}}_{\mathrm{v}})=\psi(T,\bar{\mathbf{C}},\bar{\mathbf{C}}_{\mathrm{v}})+p(J_{\mathrm{F}}-1)+q(J_{\mathrm{v}}-1)$$

given

$$\phi_{\mathrm{int}}(\mathbf{X}^0,t)=\left(\bar{\mathbf{\Pi}}(\mathbf{X}^0,t)-\rho\frac{\partial\psi(T,\bar{\mathbf{C}},\bar{\mathbf{C}}_{\mathrm{v}})}{\partial\mathbf{C}(\mathbf{X}^0,t)}-p\,\mathrm{Cof}\,\bar{\mathbf{F}}(\mathbf{X}^0,t)\right):\bar{\mathbf{F}}(\mathbf{X}^0,t)-\left(\rho\frac{\partial\psi(T,\bar{\mathbf{C}},\bar{\mathbf{C}}_{\mathrm{v}})}{\partial\bar{\mathbf{C}}_{\mathrm{v}}(\mathbf{X}^0,t)}+q\,\mathrm{Cof}\,\bar{\mathbf{C}}_{\mathrm{v}}(\mathbf{X}^0,t)\right):\dot{\bar{\mathbf{C}}}_{\mathrm{v}}(\mathbf{X}^0,t)-\rho\left(s(\mathbf{X}^0,t)+\frac{\partial\psi(T,\bar{\mathbf{C}},\bar{\mathbf{C}}_{\mathrm{v}})}{\partial T(\mathbf{X}^0,t)}\right)\dot{T}(\mathbf{X}^0,t). \quad (6)$$

However, under the definition of intrinsic dissipation in terms of the potential of dissipation [14] we also have

$$\phi_{\mathrm{int}}(\mathbf{X}^0,t)=\frac{\partial\varphi(\dot{\bar{\mathbf{C}}}_{\mathrm{v}})}{\partial\dot{\bar{\mathbf{C}}}_{\mathrm{v}}(\mathbf{X}^0,t)}:\dot{\bar{\mathbf{C}}}_{\mathrm{v}}(\mathbf{X}^0,t)\geqslant 0, \quad (7)$$

where the potential of dissipation is deduced from the rheological model such that the intrinsic dissipation remains positive or null. The latter leads to the three following relations describing the thermo-viscoelastic behaviour:

$$\bar{\mathbf{\Pi}}(\mathbf{X}^0,t)=\rho\frac{\partial\psi(T,\bar{\mathbf{C}},\bar{\mathbf{C}}_{\mathrm{v}})}{\partial\bar{\mathbf{C}}(\mathbf{X}^0,t)}+p\,\mathrm{Cof}\,\bar{\mathbf{F}}(\mathbf{X}^0,t) \quad (8)$$

$$s(\mathbf{X}^0,t)+\frac{\partial\psi(\bar{\mathbf{C}},\bar{\mathbf{C}}_{\mathrm{v}})}{\partial T}=0 \quad (9)$$

$$\rho\frac{\partial\psi(T,\bar{\mathbf{C}},\bar{\mathbf{C}}_{\mathrm{v}})}{\partial\bar{\mathbf{C}}_{\mathrm{v}}}+\frac{\partial\varphi(\dot{\bar{\mathbf{C}}}_{\mathrm{v}})}{\partial\dot{\bar{\mathbf{C}}}_{\mathrm{v}}}+q\,\mathrm{Cof}\,\bar{\mathbf{C}}_{\mathrm{v}}(\mathbf{X}^0,t)=0. \quad (10)$$

Thermal dissipation. To describe the thermal dissipation, we use Fourier law in the reference configuration written as

$$\mathbf{Q}(\mathbf{X}^0,t)=-\bar{\mathbf{K}}_{\mathrm{L}}(\mathbf{X}^0,t)\mathbf{gradT}(\mathbf{X}^0,t)$$

$$\text{with:}\quad \bar{\mathbf{K}}_{\mathrm{L}}(\mathbf{X}^0,t)=\bar{\mathbf{F}}^{-1}(\mathbf{X}^0,t)\bar{\mathbf{K}}(T)\bar{\mathbf{F}}^{-\mathrm{T}}(\mathbf{X}^0,t),$$

where $\bar{\mathbf{K}}_{\mathrm{L}}(\mathbf{X}^0,t)$ is the Lagrangian thermal con-

ductivity tensor in the reference configuration. The thermal dissipation always remains positive or null if

$$\phi_{th}(\mathbf{X}^0, t) = \mathbf{gradT}(\mathbf{X}^0, t)\bar{\mathbf{K}}_L(\mathbf{X}^0, t)\mathbf{gradT}(\mathbf{X}^0, t) \geqslant 0.$$

2.3. *Energy equation*

Using the relationship ($e = \Psi + Ts$), the time derivative of internal energy can be written as

$$\frac{de}{dt} = \frac{\partial\psi(T, \bar{\mathbf{C}}, \bar{\mathbf{C}}_v)}{dT}\frac{dT}{dt} + \frac{\partial\psi(T, \bar{\mathbf{C}}, \bar{\mathbf{C}}_v)}{\partial\bar{\mathbf{C}}} : \frac{d\bar{\mathbf{C}}}{dt} + \frac{\partial\psi(T, \bar{\mathbf{C}}, \bar{\mathbf{C}}_v)}{\partial\bar{\mathbf{C}}_v} : \frac{d\bar{\mathbf{C}}_v}{dt} + T\frac{ds(T, \bar{\mathbf{C}}, \bar{\mathbf{C}}_v)}{dt} + s\frac{dT}{dt}.$$

When substituting the above expression into the conservation of energy equation (4) and when using relations (8) and (9), we obtain if the terms are related to incompressibility are neglected

$$\rho T\frac{ds(T, \bar{\mathbf{C}}, \bar{\mathbf{C}}_v)}{dt} + \rho\frac{\partial\psi(T, \bar{\mathbf{C}}, \bar{\mathbf{C}}_v)}{\partial\bar{\mathbf{C}}_v} : \frac{d\bar{\mathbf{C}}_v}{dt} - r(\mathbf{X}^0, t) + \operatorname{div}\mathbf{Q}(\mathbf{X}^0, T) = 0. \quad (11)$$

In addition, entropy $s(T, \bar{\mathbf{C}}, \bar{\mathbf{C}}_v)$ also depends on $T, \bar{\mathbf{C}}$ and $\bar{\mathbf{C}}_v$ according to equation (9), and consequently we have

$$\frac{ds(T, \bar{\mathbf{C}}, \bar{\mathbf{C}}_v)}{dt} = \frac{\partial s(T, \bar{\mathbf{C}}, \bar{\mathbf{C}}_v)}{\partial T}\frac{dT}{dt} - \frac{\partial^2\psi(T, \bar{\mathbf{C}}, \bar{\mathbf{C}}_v)}{\partial T\partial\bar{\mathbf{C}}} : \frac{d\bar{\mathbf{C}}}{dt} - \frac{\partial^2\psi(T, \bar{\mathbf{C}}, \bar{\mathbf{C}}_v)}{\partial T\partial\bar{\mathbf{C}}_v} : \frac{d\bar{\mathbf{C}}_v}{dt}.$$

By placing the above expression in equation (11), then using equations (9) and (10) and introducing the heat capacity ($Cp = T\,\partial s/\partial T$), the energy equation for a thermo-viscoelastic material under large deformations is finally expressed as

$$\rho Cp\frac{dT(\mathbf{X}^0, t)}{dt} = -\operatorname{div}\mathbf{Q}(\mathbf{X}^0, T) + r(\mathbf{X}^0, t) + Qs(\mathbf{X}^0, T), \quad (12)$$

where the source term $Qs(\mathbf{X}^0, T)$ is given by

$$Qs(\mathbf{X}^0, t) = \frac{1}{2}T\frac{\partial\bar{\mathbf{S}}(\mathbf{X}^0, T)}{\partial T} : \frac{d\bar{\mathbf{C}}(\mathbf{X}^0, t)}{dt} - \left(T(\mathbf{X}^0, t)\frac{\partial^2\varphi}{\partial\bar{\mathbf{C}}_v\partial T} - \frac{\partial\varphi}{\partial\bar{\mathbf{C}}_v}\right) : \frac{d\bar{\mathbf{C}}_v(\mathbf{X}^0, T)}{dt}.$$

Note that when mechanical parameters do not depend on temperature, the source term becomes

$$Qs(\mathbf{X}^0, T) = \frac{\partial\varphi}{\partial\bar{\mathbf{C}}_v} : \frac{d\bar{\mathbf{C}}_v(\mathbf{X}^0, T)}{dt} = \phi_{int}(\mathbf{X}^0, t). \quad (13)$$

3. NUMERICAL MODEL

The numerical modelling of the thermo-viscoelastic problem includes two parts. The first part is the discrete formulation and its solution for the equations of mechanics by a finite element analysis and the second part is similar, but focuses on the energy equation. As the first part has already been detailed in a previous article [16], here we will only deal with the second part.

3.1. *Integral formulation*

We search for a function $T(\mathbf{X}^0, t)$ satisfying equation (12) on the domain V^0, as well as the boundary conditions on S^0. As it is an unsteady problem, this solution also has to satisfy the initial conditions. To build a discrete model by the finite element method, we adopt the classical method which introduces a polynomial approximation for each sub-domain V_e^0 in the integral form I of the weak formulation of the problem

$$I = \sum_{e=1}^{NEL}\left\{\int_{V_e^0}\rho Cp\delta T\frac{\partial T}{\partial t}dV_e^0 - \int_{V_e^0}Q_i\frac{\partial\delta T}{\partial x_i^0}dV_e^0 - \int_{V_e^0}\delta TQ_s\,dV_e^0 + \int_{S_e^0}\delta T\mathbf{QN}^0\,dS_e^0\right\}.$$

Here the test functions δT are selected in the same space as that of the trial functions $T(\mathbf{X}^0, t)$ and NEL represents the total number of elements which form a nonoverlapping covering of the domain V^0.

Boundary conditions. In the boundary integral, the expression $\mathbf{QN}^0\,dS_e^0$ is flux ϕ_e^0 passing through the surface element dS_e^0 in the reference configuration. This flux can be mapped to the deformed configuration where the boundary conditions possess physical meaning

$$\phi_e^0\,dS_e^0 = \phi_e\,dS_e,$$

where ϕ_e is the flux passing through element dS_e, which is the image in the present configuration of the surface element dS_e^0. It also follows that from equation (1b) we can demonstrate that

$$dS_e = \sqrt{\mathbf{N}^0\bar{\mathbf{F}}^{-1}\bar{\mathbf{F}}^{-T}\mathbf{N}^0}\,dS_e^0$$

and finally the relationship between the two fluxes is

$$\phi_e^0 = \sqrt{\mathbf{N}^0\bar{\mathbf{F}}^{-1}\bar{\mathbf{F}}^{-T}\mathbf{N}^0}\,\phi_e.$$

The flux ϕ_e in the current configuration consists of:

- a flux with a value imposed on surface S_{ef}: ϕ_{ef};
- a convective and/or radiative flux defined on surface S_{em} by relation

$$\phi_{em} = -(h + \varepsilon\sigma(T + T_z)(T^2 + T_z^2))(T - T_z) = f(T)(T - T_z).$$

The boundary integral finally has the following form:

$$\int_{S_e} \delta T \mathbf{Q} \mathbf{N}^0 \, dS_e = \int_{S_{ef}^0} \delta T \sqrt{\mathbf{N}^0 \bar{\mathbf{F}}^{-1} \bar{\mathbf{F}}^{-T} \mathbf{N}^0} \, \phi_{ef} \, dS_{ef}^0 + \int_{S_{em}^0} \delta T f(t) \sqrt{\mathbf{N}^0 \bar{\mathbf{F}}^{-1} \bar{\mathbf{F}}^{-T} \mathbf{N}^0} (T - T_\infty) \, dS_{em}^0$$

where the surface elements dS_{ef}^0 and dS_{em}^0 are, respectively, the images of the surface elements dS_{ef} and dS_{em} in the present configuration on which the fluxes ϕ_{ef} and ϕ_{em} are applied.

3.2. *Matrix formulation*

Introducing the finite element approximation into the integral form leads to the following matrix form:

$$I = [M]\{\dot{T}\} + [K]\{T\} - \{VF\} \tag{14}$$

where $\{T\}$ is the vector of temperature values at the mesh nodes and $\{\dot{T}\}$ the vector of their time derivatives. The mass matrix $[M]$, the stiffness matrix $[K]$ and the body force $\{VF\}$ are obtained by assembling elementary matrices and vectors

$$[M] = \sum_{e=1}^{NEL} [M_e].$$

$$[K] = \sum_{e=1}^{NEL} ([K_e^d] + [K_e^m])$$

$$\{VF\} = \sum_{e=1}^{NEL} (\{V_e^p\} - \{V_e^m\} - \{V_e^f\}),$$

with

$$[M_e] = \int_{V_e^0} \rho C p \{N_e\} \langle N_e \rangle \, dV_e^0$$

$$[K_e^d] = \int_{V_e^0} \left\{ \frac{\partial N_e}{\partial x^0} \right\} \bar{\mathbf{K}}_L(\mathbf{X}^0, t) \left\langle \frac{\partial N_e}{\partial x^0} \right\rangle dV_e^0$$

$$[K_e^m] = \int_{S_{em}^0} f(T) Js(\mathbf{X}^0, t) \{N_e\} \langle N_e \rangle \, dS_{em}^0$$

$$\{V_e^p\} = \int_{V_e^0} \{N_e\} Q_S(\mathbf{X}^0, T) \, dV_e^0$$

$$\{V_e^f\} = \int_{S_{ef}^0} \{N_e\} \phi_{rf} Js(\mathbf{X}^0, t) \, dS_{ef}^0$$

$$\{V_e^m\} = \int_{S_{em}^0} \{N_e\} f(T) T_\infty Js(\mathbf{X}^0, t) \, dS_{em}^0.$$

The large deformation aspect of the problem enters into the stiffness matrix through the conductivity tensor $\bar{\mathbf{K}}_L(\mathbf{X}^0, t)$ previously defined. It also enters in the elementary matrices and vectors through the Jacobian $Js(\mathbf{X}^0, t)$

$$Js(\mathbf{X}^0, t) = \sqrt{\mathbf{N}^0(\mathbf{X}^0, t) \bar{\mathbf{F}}^{-1}(\mathbf{X}^0, t) \bar{\mathbf{F}}^{-T}(\mathbf{X}^0, t) \mathbf{N}^0(\mathbf{X}^0, t)}.$$

Note that the matrix $\bar{\mathbf{K}}_L(\mathbf{X}^0, t)$ and the Jacobian $Js(\mathbf{X}^0, t)$ must be computed at each Gaussian point according to the displacement of the element nodes resulting from the solution of the equations of mechanics [16].

The differential equation system (14) results in a system of nonlinear algebraic equations by using an implicit Eulerian time integration scheme. A Newton–Raphson method is used to solve the obtained nonlinear system of equations.

4. APPLICATIONS

In order to validate our approach, we have studied a two-layer elastomer-steel test piece subjected to a shear force (Fig. 2). The elastomer we use is a dimethyl–vinyl–siloxan elastomer from Rhône-Poulenc which has been vulcanized by peroxide. Under the assumption of plane and homogeneous deformations, the mechanical problem [equations (8)–(10)] has an analytical solution which allows us to use it as a benchmark for thermal modelling.

A sinusoidal displacement is applied to the central bar while the outer bars of the test piece are fixed. The characteristics of this excitation are:

- amplitude: $\Delta L = 0.5e$
- frequency: $f = \omega/2\pi = 4.5$ Hz.

The test piece is then put into a thermal enclosure with quiescent air at a temperature of 28°C. During the tests, a forced convection heat transfer occurs between air and the test piece because of the displacement imposed on the bars. To take this phenomenon into account the average heat transfer coefficient h was set at 5 W m^{-2} K^{-1} in the numerical model.

Thermocouples have been inserted into the elastomer in order to compare the predictions of the numerical model with experimental results. These thermocouples are positioned in parallel to the bars and orthogonal to their displacement direction. This prevents mechanical stresses from interfering with the measurements. Figure 3 shows on a half cross-section the dimensions of the test piece, as well as the position of the thermocouples.

We use type K thermocouples of 0.2 diameter. They are calibrated with two thermostatic baths. The first bath is maintained at 0°C (cold source), the second bath is at a temperature varying between 0 and 100°C (hot source). The temperature accuracy of both baths is about 0.1°C.

Solution of the mechanical problem—determination of the source term

For the description of the viscoelastic behaviour of the elastomer, we have used a rheological model proposed by Sidoroff [10, 17, 19] and represented on Fig. 4. It is a Poynting–Thomson model extended to large deformations and based on the principle of

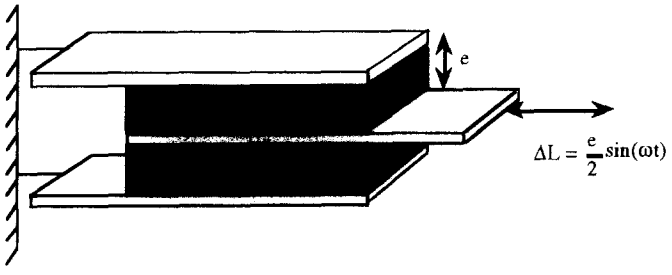

Fig. 2. Two-layer test piece submitted to a shear force when displacement is imposed.

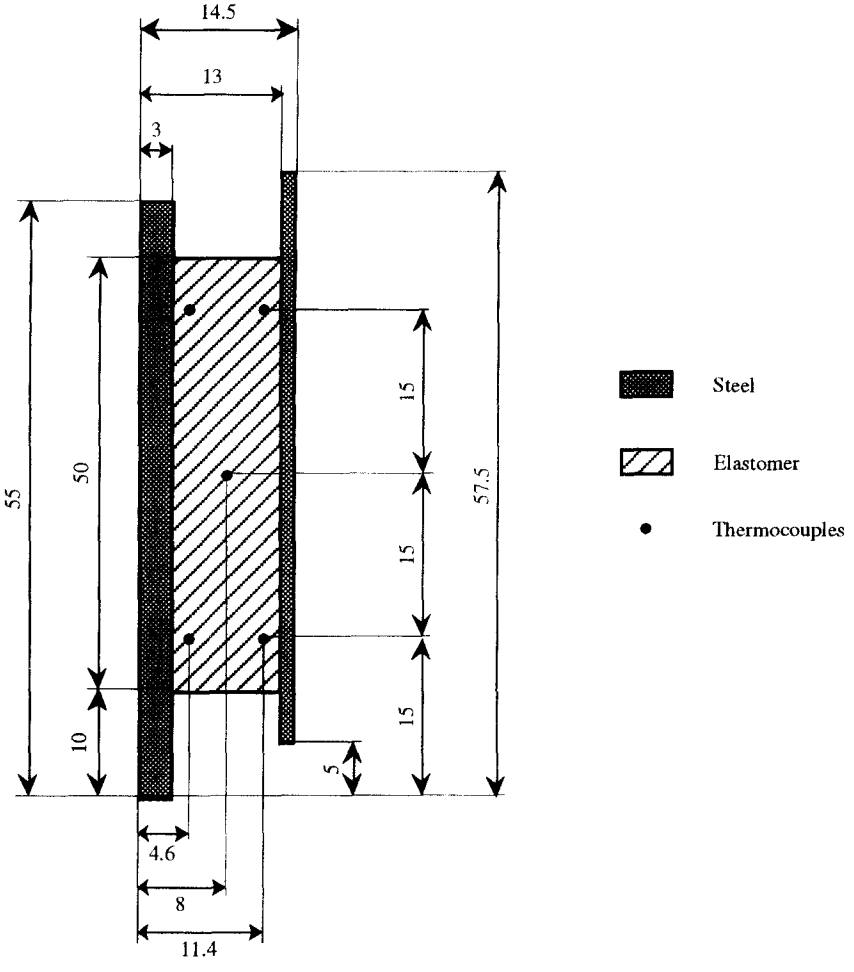

Fig. 3. Test piece dimensions and position of the thermocouples.

multiplicative decomposition of the deformations we have presented in Section 2.2.

This model is obtained by the simultaneous application of a spring and a dashpot. The whole system is assembled in series with another spring. The dominance of the hyperelastic behaviour of elastomers compared with their viscous behaviour justifies this choice. This model favours the instantaneous response of the first spring in comparison with the delayed response of the whole spring-damping system. The deformation energies of the first and second springs are given by, respectively, Hart-Smith [20] and Neohooke [21] laws

first spring—Hart-Smith law

$$\rho\Psi_1 = c_1 \int \exp\left(c_3(I_1^e - 3)^2\right) \mathrm{d}I_1^e + c_2 \,\mathrm{Ln}\frac{I_2^e}{3}$$

second spring—Neohooke law

$$\rho\Psi_2 = a_1(I_1^v - 3).$$

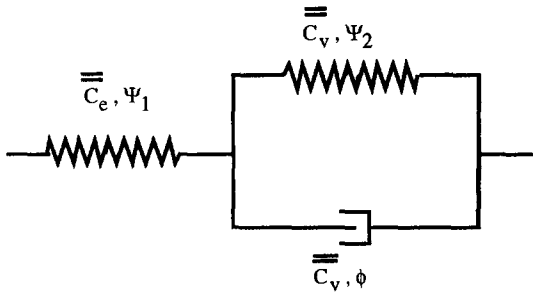

Fig. 4. Rheological model describing the elastomer behaviour.

In the previous expressions I_1^e, I_2^e and I_1^v are the invariants of the tensors $\bar{\mathbf{C}}_e$ and $\bar{\mathbf{C}}_v$. The parameters a_1, c_1, c_2, c_3 and v are determined by experiments in dynamic deformations. For a 4.5 Hz frequency and an amplitude of the deformation amounting to 50% of the elastomer thickness, we obtain

$$a_1 = 0.1 \text{ MPa}, \quad c_1 = 0.34 \text{ MPa},$$

$$c_2 = -0.065 \text{ MPa}, \quad c_3 = 5, \quad v = 0.05 \text{ MPa}.$$

On the other hand we assume with this model that the mechanical behaviour of the elastomer is temperature independent. The source term $Qs(\mathbf{X}^0, T)$ then equals to intrinsic dissipation ϕ_{int} [see equation (13)]. When taking the following function for the energy dissipation of the dashpot

$$\frac{\partial \varphi}{\partial \dot{\bar{\mathbf{C}}}_v} = v\dot{\bar{\mathbf{C}}}_v$$

this source term becomes

$$Qs(\mathbf{X}^0, t) = \phi_{\text{int}}(\mathbf{X}^0, t) = v\text{Tr}(\dot{\bar{\mathbf{C}}}_v^2).$$

Furthermore, equations (8) and (10) are written as [19]

$$\bar{\mathbf{\Pi}} = 2\rho\left(\frac{\partial \Psi_1}{\partial I_1^e}\bar{\mathbf{F}}\bar{\mathbf{P}} + \frac{\partial \Psi_1}{\partial I_2^e} \times ((\bar{\mathbf{P}}:\bar{\mathbf{C}})\bar{\mathbf{F}}\bar{\mathbf{P}} - \bar{\mathbf{F}}\bar{\mathbf{P}}\bar{\mathbf{C}}\bar{\mathbf{P}})\right) + p\,\text{Cof}\,\bar{\mathbf{F}} \quad (15)$$

$$\rho\left(-\frac{\partial \Psi_1}{\partial I_1^e}\bar{\mathbf{P}}\bar{\mathbf{C}}\bar{\mathbf{P}} + \frac{\partial \Psi_1}{\partial I_2^e}\bar{\mathbf{P}}(-(\bar{\mathbf{P}}:\bar{\mathbf{C}})\bar{\mathbf{C}} + \bar{\mathbf{C}}\bar{\mathbf{P}}\bar{\mathbf{C}})\bar{\mathbf{P}} + \frac{\partial \Psi_2}{\partial I_1^v}\bar{\mathbf{I}}\right) + v\dot{\bar{\mathbf{C}}}_v + q\,\text{Cof}\,\bar{\mathbf{C}}_v \quad (16)$$

where we have set $\bar{\mathbf{P}} = \bar{\mathbf{C}}_v^{-1}$.

Under the assumption of plane and homogeneous deformations one has

$$\bar{\mathbf{F}} = \begin{bmatrix} 1 & \gamma & 0 \\ 0 & 1 & 0 \\ 0 & 0 & 1 \end{bmatrix} \quad \text{with } \gamma = \frac{\Delta L}{e} \quad \bar{\mathbf{F}}_v = \begin{bmatrix} 1 & \gamma_v & 0 \\ 0 & 1 & 0 \\ 0 & 0 & 1 \end{bmatrix}$$

$$\bar{\mathbf{\Pi}} = \begin{bmatrix} \pi_{xx} & \pi_{xy} & 0 \\ \pi_{xy} & \pi_{yy} & 0 \\ 0 & 0 & \pi_{zz} \end{bmatrix}$$

$$\bar{\mathbf{C}}_v = \begin{bmatrix} 1 & \gamma_v & 0 \\ \gamma_v & 1+\gamma_v^2 & 0 \\ 0 & 0 & 1 \end{bmatrix} \quad \bar{\mathbf{C}}_e = \begin{bmatrix} 1 & \gamma-\gamma_v & 0 \\ \gamma-\gamma_v & 1+(\gamma-\gamma_v)^2 & 0 \\ 0 & 0 & 1 \end{bmatrix}$$

where γ_v, the relative deformation resulting from viscous effects, is the unknown of equation (16). These matrices help us deduce the following expressions for the derivatives of Ψ_1 and Ψ_2, which enter relations (15) and (16) [16]

$$\rho\frac{\partial \Psi_1}{\partial I_1^e} = c_1 \exp(c_3(I_1^e - 3)^2) = c_1 \exp(c_3(\gamma-\gamma_v)^4)$$

$$\rho\frac{\partial \Psi_1}{\partial I_2^e} = \frac{c_2}{I_2^e} = \frac{c_2}{3+(\gamma-\gamma_v)^2}$$

$$\rho\frac{\partial \Psi_2}{\partial I_1^v} = a_1.$$

After solving equation (16) with an Eulerian time integration scheme [16, 19], one obtains the evolution of the intrinsic dissipation displayed in Fig. 5. The excitation expressed by the relative sinusoidal deformation of the test piece $\gamma = \Delta L/e$ has also been displayed in this figure.

We notice that heat production varies in a sinusoidal way at a frequency which is double that of the excitation (9 Hz). This comes from the fact that the source term $Qs(\mathbf{X}^0, T)$ varies with the square of the deformation velocity. Furthermore, during the first three deformation cycles, the amplitude of the dissipation varies and oscillates periodically. This phenomenon is explained by the fact that when exerting a horizontal displacement on the central bar the entangled molecular chains are forced to 'unfold' and extend in the displacement direction. A periodic horizontal displacement causes periodic extensions and compressions of the molecular chains. This displacement of the molecular chains enables the material to progressively gain some flexibility. Furthermore, dissipation is stronger in the direction of the displacement rather than in the reverse direction. This comes from the fact that after forcing the molecular chains to extend in a direction, they are forced to extend in the reverse direction. Such a phenomenon has been observed previously by the authors and is known as the Mullins effect [22]. After the fourth cycle, the amplitude of the response in dissipation is quasi-steady and the heat production can then be written as

$$Qs(\mathbf{X}^0, T) = Qs(t) = 176\,500(1+\sin(18\pi t)) + 7400. \quad (17)$$

4.1. *Numerical modelling of the thermal problem*

The solution of the energy equation (12) associated with the shearing test can be carried out on half of the

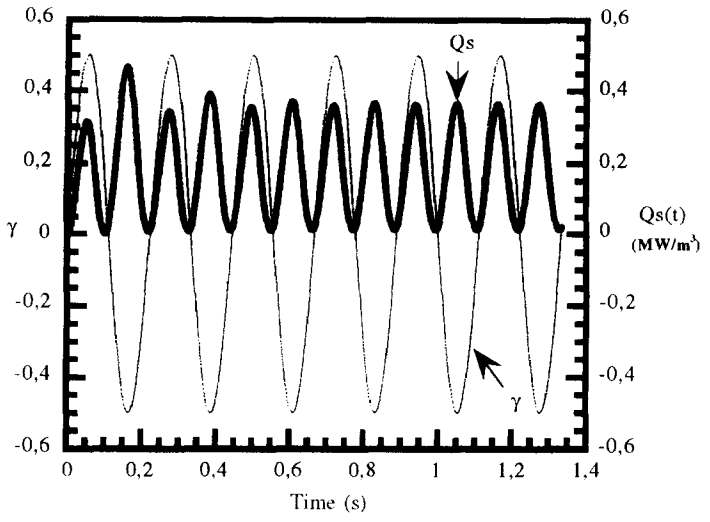

Fig. 5. Variation of heat production with respect to time.

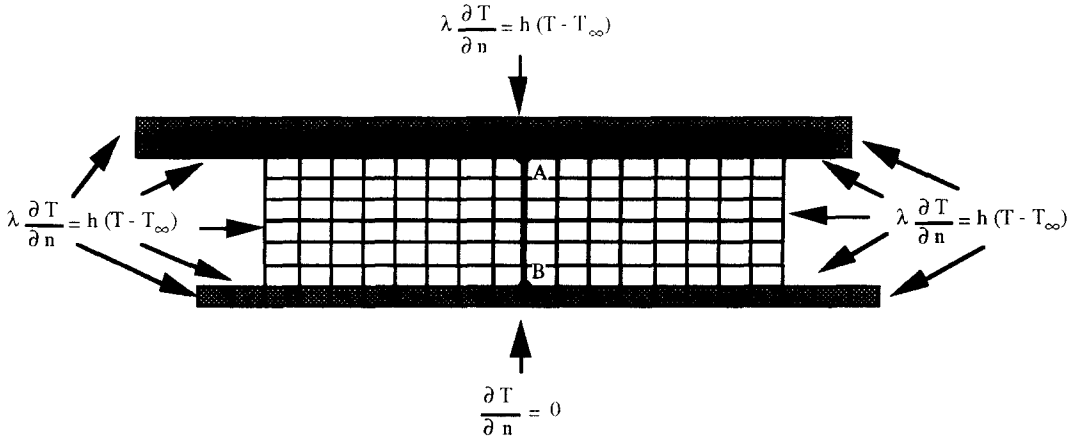

Fig. 6. Computational mesh and boundary conditions for the test-piece.

cross-section of the test-piece because of symmetry. The numerical model described in Section 3 was implemented with a variable source term such as the one displayed in Fig. 5 for the first three cycles and then equation (17) was used. The mesh, shown in Fig. 6, is made up of 165 isoparametric Q4 elements of Lagrangian type, 55 linear elements L2 and contains 284 nodes. The 69 Q4 elements in dark represent the steel bars and the other 96 represent the elastomer. A zero flux condition is applied on the symmetry axis and a convective heat transfer condition is imposed on the other mesh boundaries, with an average heat transfer coefficient h of 5 W m^{-2} K^{-1} and an ambient temperature T_∞ of 28 C.

The values of thermophysical properties of the materials are: for steel: $\lambda = 45$ W m^{-1} K^{-1} and $\rho Cp = 3.5 \times 10^6$ J m^{-3} K^{-1} and for the elastomer: $\lambda = 0.127$ W m^{-1} K^{-1} and $\rho Cp = 1.33 \times 10^6$ J m^{-3} K^{-1}.

The numerical computation was carried out for 660 s, namely 3000 cycles. Each cycle is divided into 20 time steps of 0.0111 s.

Figure 7 compares the evolution of the numerical results with the experimental ones in the centre of the elastomer.

4.2. *Explanation of the obtained results*

We notice that the temperature in the centre increases rather rapidly at the beginning. Indeed, up to the 110th cycle, the evolution is almost linear with a 0.08 C increase per cycle. It then evolves more slowly and tends asymptotically towards a temperature of about 70 C. The total increase in temperature amounts to 42 C. This increase would obviously be larger if the amplitude or frequency of the excitation signal were increased.

The curves displayed in Fig. 7 show a large difference between the results of the numerical model and the experimental ones. Therefore, the assumption that thermo-mechanical parameters and consequently the source term do not depend on temperature must be questioned. When shearing forces generate a large stress friction in the molecular chains, this assumption is only valid as a first approximation. Thus, when the

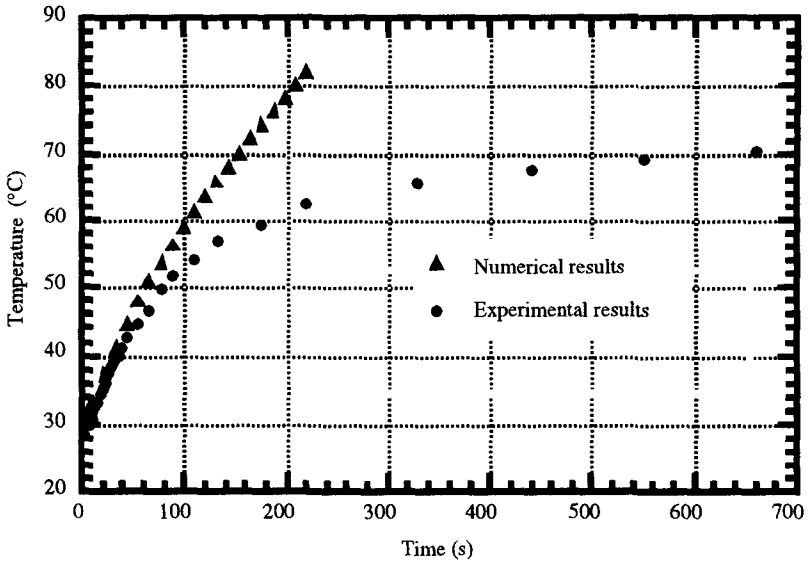

Fig. 7. Comparison of the numerical results with the experimental ones in the centre of the elastomer.

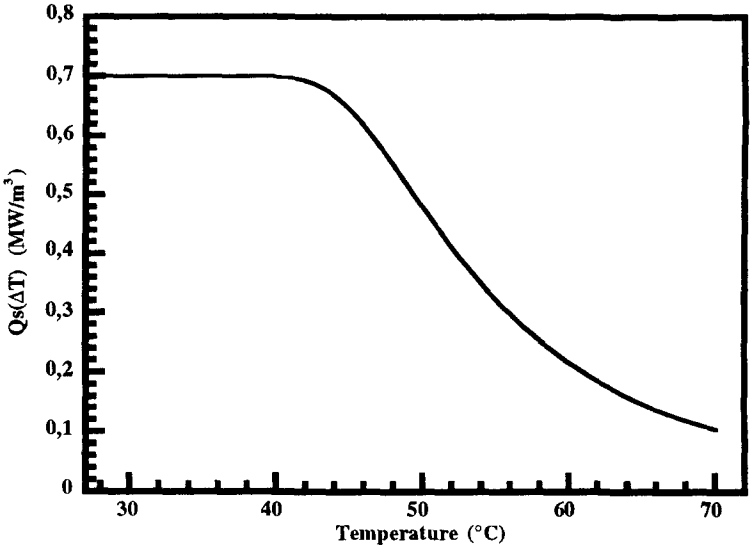

Fig. 8. Evolution of the source term as a function of temperature.

real behaviour of the material needs to be described more precisely, it is necessary to consider that the heat production depends not only on the mechanical forcing, but also on the temperature, even though it is far from the glass transition.

To assess this dependence, the experimental temperature measurements have been used to determine the evolution of the source term with respect to temperature by utilizing an inverse method of Beck type [23]. The detailed calculations and computations are presented in Bérardi's thesis [24]. The obtained results represented on Fig. 8 show that this evolution follows a law of Arrhenius type

$$Qs(T) = 0.7\left(1-\exp\left(-\frac{15670}{(T-Ti)^{3.07}}\right)\right), \quad (18)$$

where Ti is the initial temperature of the elastomer.

This curve shows that the heat production within the elastomer is at first constant, then decreases with respect to temperature. A softening phenomenon of the material can explain this result. Furthermore, in the initial cycles of forcing, the movement of the entangled molecular chains produced an additional energy dissipation.

The function in equation (18) was implemented in our numerical model. Figure 9 compares the evolution with respect to time of the temperatures resulting from the numerical computation with the experimental values. The figure shows a good agreement between the results. The difference between the numerical and experimental results can be explained by a lack of accuracy when determining the heat transfer coefficient. The comparison of the numerical results with the experimental ones given by the other

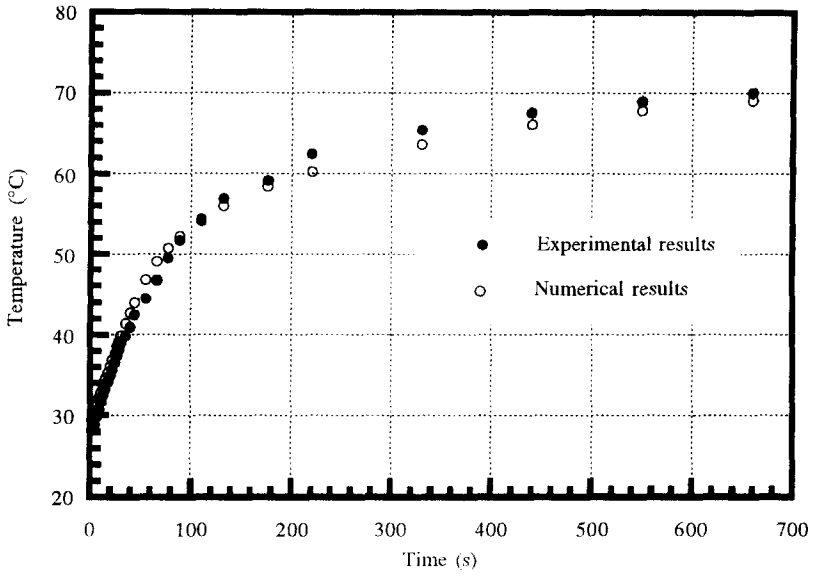

Fig. 9. Comparison of the numerical results using the inverse method with the experimental ones in the centre of the elastomer.

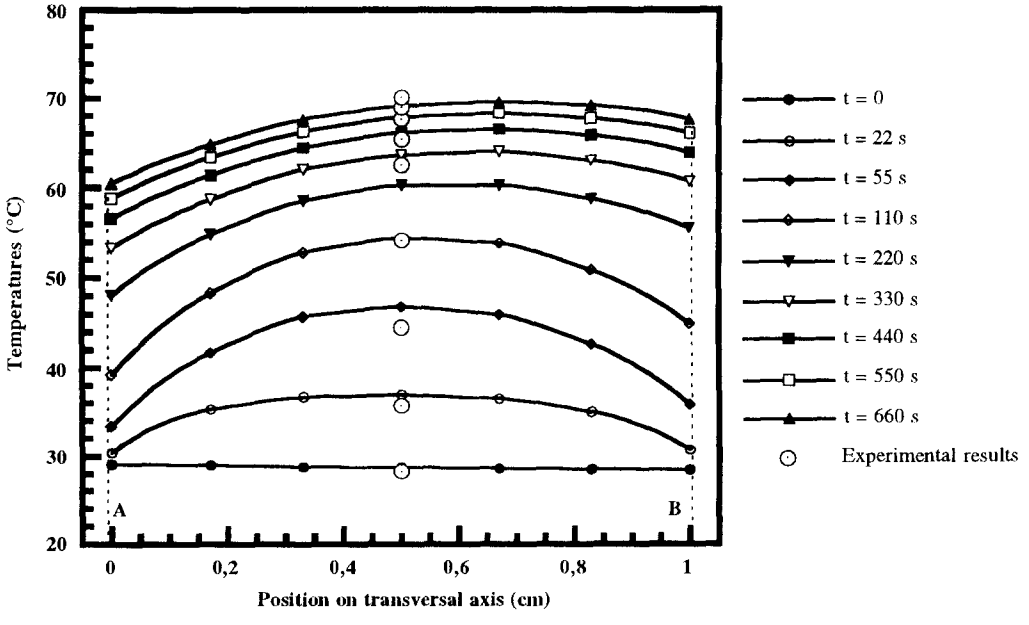

Fig. 10. Evolution of the transverse temperature field of the test-piece with respect to the number of cycles.

thermocouples is totally similar to the comparison presented on Fig. 9. It appears that the evolution of the source term according to temperature is well represented by equation (18).

Figure 10 shows the evolution of the temperature field on line AB (see Fig. 6) as a function of the number of cycles.

As previously, we can note that this temperature field evolves rapidly during the initial forcing cycles. This generates a rather large temperature gradient in the elastomer. Besides, the flux exchanged by convection around the test piece imposes a temperature maximum at first situated in the centre of the elastomer and then moves towards the symmetry axis of the test piece. This phenomenon is illustrated in Fig. 11 through the use of isotherms within the test piece at various time intervals.

The appearing hot zone can occur in many industrial applications related to more complex composite structures. On the other hand, this phenomenon will be more important when the deformation amplitude and the excitation frequency are higher. This will enhance the damaging phenomena strongly related to the appearance of hot spots. This could also involve a shorter lifetime of parts of the structures [25, 26].

Finally, the rheological model used cannot give

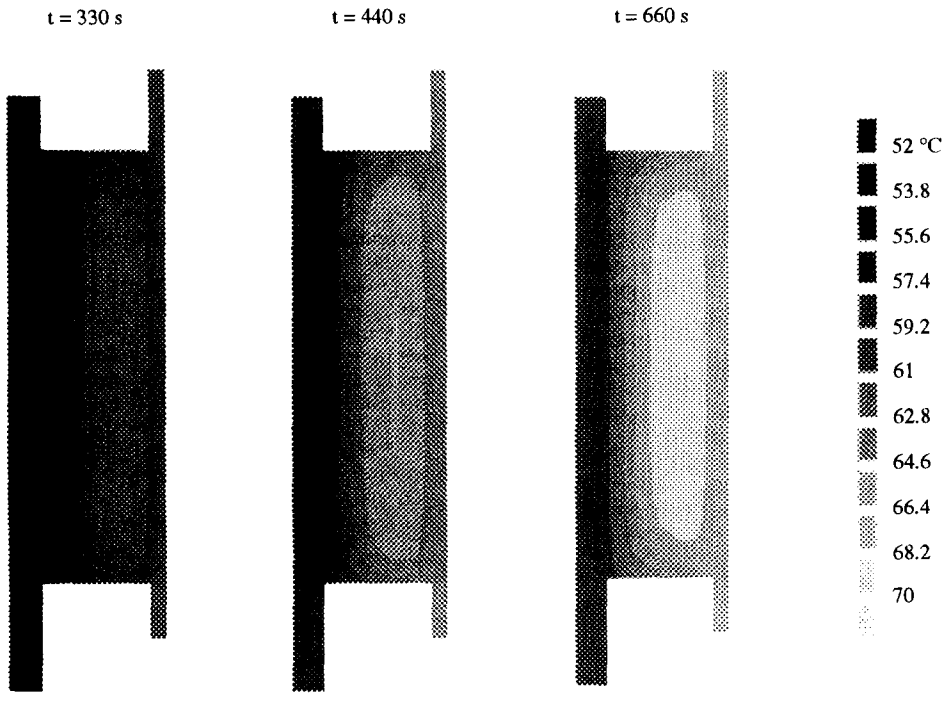

Fig. 11. Evolution of the temperature field with respect to time.

results close enough to reality, since it assumes that the thermo-mechanical parameters and the source term are temperature independent. It is therefore necessary to develop other models, with the results obtained through inverse method. These models should consider the behaviour dependence of the material with respect to temperature.

CONCLUSION

In this article we have presented an approach to obtain equations for a thermo-viscoelastic coupling with large deformations. The equations are written in Lagrangian form in the reference configuration. Among them, the energy equation contains a source term depending upon the viscous dissipation in the mechanical behaviour model. Assuming that this source term is temperature independent, a solution of this equation via finite element analysis was carried out for a two-layer test piece subjected to a plane and homogeneous shearing force.

In order to validate the results from the rheological model, an experimental assembling was implemented. In this assembling, the thermocouples enable us to measure the rise of temperature at various points of the elastomer. The experimental results are then compared with the results of the numerical model. They show that the assumption of a temperature independent source term can only be a first approximation. When a more accurate description of the real behaviour of the material is required, it then becomes necessary to consider the variation of the source term with temperature, even far from the glass transition temperature. An expression for the source term variation with temperature was determined by an inverse method. The numerical results obtained with this function agree much better with the experimental results. They emphasize that the material becomes softer during the initial cycles of the response in heat production when subjected to a harmonic mechanical excitation of amplitude amounting to 50% of the test piece thickness and of frequency 4.5 Hz. This computation has also demonstrated the existence of a strong gradient within the elastomer which causes the formation of a hot zone within it. This zone will be crucial in industrial applications as it increases the damaging phenomena.

The obtained results should help identify a rheological model whose coefficients are temperature dependent.

Acknowledgements—The authors would like to thank Professor R. L. Sani for his advice about the writing of our paper.

REFERENCES

1. I. P. Borodin and T. N. Khazanovitch, The strain dependence of elastomer loss modulus. Rubber elasticity and the structure of polymer networks, *Polymer* **27**, 28–37 (1986).
2. G. W. M. Peters, Differential models for thermo-rheological modelling of viscoelastic materials, *IUTAM Symposium*, Kerkrade, The Netherlands, November (1993).
3. K. N. Morman, Original contributions. An adaptation of finite linear viscoelasticity theory for rubber-like viscoelasticity by use of the generalized strain measure, *Rheologica Acta* **27**, 3–14 (1988).

4. V. G. Karnaukhov, B. P. Gumenyuk and V. I. Kozlov, Numerical study of thermomechanical behavior of viscoelastic bodies in plane harmonic deformation, translated from *Prikladnaya Mekh.* **21,** 10–16 (1985).
5. I. K. Senchenkov, V. G. Karnaukhov and V. I. Kozlov, Toward a theory of governing equations of nonlinear thermoviscoelasticity for periodic deformation, translated from *Prikladnaya Mekh.* **21,** 97–104 (1986).
6. V. I. Kozlov and V. G. Karnaukhov, Finite element method of studying the thermomechanical behavior of viscoelasticity solids of revolution under cyclic loading, translated from *Prikladnaya Mekh.* **19,** 40–45 (1983).
7. V. V. Kirichevekii and B. M. Dokhnyak, Thermomechanics of structures made of elastomers in cyclic loading on the basis of finite element model, translated from *Problemy Prochnosti* **10,** 74–82 (1989).
8. H. R. Srinatha and R. W. Lewis, A finite element method for thermoviscoelastic analysis of plane problems, *Comput. Meth. Appl. Mech. Engng* **25,** 21–33 (1981).
9. J. T Oden and W. H. Armstrong, Analysis of nonlinear dynamic coupled thermoviscoelasticity problems by the finite element method, *Comput. Struct.* **1,** 603–621 (1971).
10. F. Sidoroff, Un modèle viscoélastique nonlinéaire avec configuration intermédiaire, *J. mécanique* **13,** 679–713 (1974).
11. P. Le Tallec, K. Hanna, F. E. Jouve and A. Kaiss, Viscoelastic model for the human cornea, *High Perform. Comput.* **2,** (1991).
12. F. Sidoroff, Cours sur les grandes déformations, Ecole d'été Sophia-Antipolis, rapport GRECO 51 (1982).
13. J. Lemaitre and J. L. Chaboche, *Mécanique des Matériaux Solides* (1st Edn.), Dunod, Paris (1988).
14. P. Germain, *Mécanique* (2nd Edn.), Ellipses, Paris (1986).
15. C. Rahier, Analyse numérique du roulage stationnaire de structures viscoélastiques non linéaires en grandes déformations, Thèse de doctorat, Université de Paris 6 (1991).
16. C. Carpentier, G. Bérardi and A. Boukamel, Modélisation du comportement thermo-mécanique d'un matériau viscoélastique non linéaire en grandes déformations, *Proceedings of the Strucome* 93, pp. 579–589 (1993).
17. P. Le Tallec and C. Rahier, Numerical models of steady rolling for non-linear viscoelastic structures for finite deformations, *Int. J. Numer. Meth. Engng* **37,** 1159–1186 (1994).
18. J. Lubliner, A model of rubber viscoelasticity, *Mech. Res. Comm.* **12,** 93–99 (1985).
19. C. Carpentier, J. E. Brunel and A. Boukamel, Modélisation du comportement thermo-mécanique d'un matériau viscoélastique non linéaire en grandes déformations, *Proceedings of the Centenaire ESIM*, pp. 68–78 (1993).
20. L. J. Hart-Smith, Elasticity parameters for finite deformations of rubber-like materials, *J. Appl. Math. Phys.* **17,** 608–626 (1966).
21. L. Treolar, *The Physics of Rubber Elasticity*. Clarendon Press, Oxford (1958).
22. J. A. C. Harwood and L. Mullins, Stress softening in natural rubber vulcanizates. Part II Stress softening effects in pure gum and filler loaded rubbers, *J. Appl. Polym. Sci.* **9,** 3011–3021 (1965).
23. J. V. Beck, *Inverse Heat Conduction—Ill Posed Problems* (1st Edn). Wiley-Interscience, New York (1985).
24. G. Bérardi, Modélisation numérique du comportement thermo-viscoélastique d'un élastomère en grandes déformations, Thèse de doctorat, Université de Provence (1995).
25. A. N. Gent, *The Mechanism of Fracture*, Vol. AMD 19. ASME, New York (1976).
26. E. J. Kramer, Microscopic and molecular fundamentals of crazing, in *Advances in Polymer Science*, Vol. 52/53, pp. 1–56. Springer, Berlin.